Evaluation of Orbit Errors and Measurement Corrections in Differential Navigation With LEO Satellites

Joe Saroufim, Samer Hayek, and Zaher M. Kassas
The Ohio State University

BIOGRAPHY

Joe Saroufim is a Ph.D student in the Department of Electrical and Computer Engineering at The Ohio State University and a member of the Autonomous Systems Perception, Intelligence, and Navigation (ASPIN) Laboratory. He received a B.E. in Mechanical Engineering from the Lebanese American University. His current research interests include low Earth orbit satellites, situational awareness, autonomous vehicles, and sensor fusion.

Samer Hayek is a Ph.D student in the Department of Electrical and Computer Engineering at The Ohio State University and a member of the ASPIN Laboratory. He received a B.E. in Mehchanical Engineering from the Lebanese American University. His current research interests include low Earth orbit satellites, autonomous vehicles, sensor fusion, and simultaneous localization and mapping.

Zaher (Zak) M. Kassas is a professor at The Ohio State University and TRC Endowed Chair in Intelligent Transportation Systems. He is the Director of the Autonomous Systems Perception, Intelligence, and Navigation (ASPIN) Laboratory. He is also director of the U.S. Department of Transportation Center: CARMEN (Center for Automated Vehicle Research with Multimodal AssurEd Navigation), focusing on navigation resiliency and security of highly automated transportation systems. He received a B.E. in Electrical Engineering from the Lebanese American University, an M.S. in Electrical and Computer Engineering from The Ohio State University, and an M.S.E. in Aerospace Engineering and a Ph.D. in Electrical and Computer Engineering from The University of Texas at Austin. He is a recipient of the National Science Foundation (NSF) CAREER award, Office of Naval Research (ONR) Young Investigator Program (YIP) award, Air Force Office of Scientific Research (AFOSR) YIP award, IEEE Walter Fried Award, Institute of Navigation (ION) Samuel Burka Award, and ION Col. Thomas Thurlow Award. He is an Associate Editor of the IEEE Transactions on Aerospace and Electronic Systems and the IEEE Transactions on Intelligent Transportation Systems. He is a Fellow of the ION and a Distinguished Lecturer of the IEEE Aerospace and Electronic Systems Society. His research interests include cyber-physical systems, navigation systems, and intelligent transportation systems.

ABSTRACT

Ephemeris errors and measurement corrections in differential navigation with low Earth orbit (LEO) space vehicles (SVs) are analyzed. First, orbit errors are characterized for the non-differential case, showing the dependency of the range measurement errors on the receiver-to-SV geometry. The study is then extended to the differential case, where the maximum differential range error is found to occur when the baseline is normal to the projected measurement vector from one receiver onto the local navigation frame. A simulation study is presented to assess the differential navigation performance with 14 Starlink and 11 OneWeb LEO satellites. The framework fused differenced pseudorange measurements from a base and rover to LEO SVs with inertial measurement unit (IMU) measurements via an extended Kalman filter (EKF) in a tightly-coupled fashion to estimate the rover's states. The simulation considered an aerial vehicle equipped with a tactical-grade IMU, an altimeter, a GNSS receiver, and a LEO receiver making pseudorange measurements to the LEO SVs. During 300 seconds of flight time, the vehicle traveled a distance of 28 km, the last 23 km of which were without GNSS, achieving a three-dimensional (3-D) position root mean squared error (RMSE) of 52 cm, compared to 12.5 m using the non-differential framework. Experimental results are presented, showing the potential of differential navigation in reducing ephemeris, clocks, and atmospheric errors. A ground vehicle traversed a distance of 540 m in 60 seconds, the last 492 m of which without GNSS signals, while making Doppler measurements to 2 Orbcomm and 1 Iridium LEO SVs, whose ephemerides were obtained from two-line element (TLE) files, propagated with simplified general perturbation 4 (SGP4) orbit propagator. The differential framework yielded a position RMSE of 7.13 m, compared to 41.29 m using non-differential measurements, and 87.74 m with GNSS-aided IMU.

I. INTRODUCTION

Existing low Earth orbit (LEO) satellite constellations, each of which totaling less than a hundred satellites (e.g., Orbcomm, Globalstar, Iridium NEXT), are being joined by megaconstellations of LEO satellites, each of which comprising up to thousands

of LEO satellites (e.g., OneWeb, Starlink, Project Kuiper). SpaceX is currently dominating these megaconstellations with about 4,000 functioning Starlink space vehicles (SVs) in LEO, with a possible extension to 42,000. Uninterrupted signals from these satellites will soon cover the Earth, heralding a new age for opportunistic position, navigation, and timing (PNT) (Kassas et al., 2019; Jardak and Jault, 2022; Janssen et al., 2023; Menzione and Paonni, 2023; Prol et al., 2023).

Conventional navigation methods that rely on fusing global navigation satellite system (GNSS) receivers with inertial measurement units (IMUs) raise alarming concerns when GNSS signals become unavailable or unreliable due to (i) intentional jamming (Miralles et al., 2020) or spoofing (Bhatti and Humphreys, 2017), (ii) signal obstruction and multipath in deep urban canyons (McGraw and Braasch, 1999), and (iii) unintentional interference (Hegarty et al., 2020), leading to unbounded accumulation of IMU errors.

To address the shortcomings of GNSS, opportunistic navigation using terrestrial signals of opportunity (SOPs) has been studied extensively, achieving lane-level positioning on ground vehicles (Peral-Rosado et al., 2016; Maaref et al., 2019; Whiton et al., 2022), and sub-meter-level accuracy on unmanned aerial vehicles (UAVs) (Khalife and Kassas, 2022). The boom in LEO satellites has attracted researchers' attention in recent years towards exploiting LEO signals for PNT in either a standalone fashion (Khalife et al., 2022; Huang et al., 2022; Zhao et al., 2022) or an IMU aiding fashion (Kassas et al., 2019; Farhangian et al., 2021).

Besides their large abundance around the Earth, several desirable characteristics qualify LEO SVs as promising PNT sources (Prol et al., 2022): (i) being twenty times closer to Earth than GNSS SVs that reside in medium Earth orbit (MEO) satellites results in higher received carrier-to-noise ratio, (ii) residing at different altitudes ranging from 160 to 1,000 km with different orbit orientations offers favorable geometric dilution of precision for accurate position and velocity estimation (Kennewell and Vo, 2013), and (iii) orbiting at high speed compared to MEO SVs yields more informative Doppler measurements.

However, exploiting broadband LEO satellite SOPs for navigation purposes comes with challenges, as they are owned by private operators that typically do not disclose crucial information about the satellites': (i) ephemerides, (ii) clock synchronization and stability, and (iii) signal specifications. Several studies have been published over the past few years to address satellite orbit, clock, and propagation errors (Kozhaya et al., 2021; Khairallah and Kassas, 2021; Morton et al., 2022; Cassel et al., 2022; Wang et al., 2023; Zhao et al., 2023; Wu et al., 2023; Jiang et al., 2023a; Ye et al., 2023; Khalife and Kassas, 2023; Saroufim et al., 2023; Kassas et al., 2023a); receiver and signal design (Tan et al., 2019; Wei et al., 2020; Bilardi, 2021; Orabi et al., 2021; Kassas et al., 2021; Neinavaie et al., 2022; Egea-Roca et al., 2022; Huang et al., 2022; Pinell et al., 2023; Yang et al., 2023; Humphreys et al., 2023; Yang and Soloviev, 2023); and navigation framework design (Farhangian et al., 2021; Psiaki, 2021; Hartnett, 2022; Singh et al., 2022; Jiang et al., 2022; More et al., 2022; Shi et al., 2023; Guo et al., 2023; Kanamori et al., 2023; Sabbagh and Kassas, 2023; Farhangian and Landry, 2023; Ries et al., 2023).

Although LEO SVs typically do not transmit their position in their downlink signals, they may be calculated from the publicly available two-line element (TLE) sets published and updated daily by the North American Aerospace Defense Command (NORAD). The first line in the TLE contains designation and temporal data, whereas the second line consists of a list of the standard orbital elements (inclination angle, right ascension of ascending node, eccentricity, argument of perigee, mean anomaly, and mean motion) defined at a certain time epoch. Using this information, orbit determination algorithms, such as simplified general perturbation 4 (SGP4), can be used to estimate any LEO SV's ephemeris (Vallado and Crawford, 2008). Nonetheless, although SGP4 takes into account atmospheric drag and satellites perturbations, its corresponding propagated TLE ephemeris results in state error ranging from hundreds of meters to a few kilometers, mostly concentrated in the tangential or along-track axis of the LEO satellite's body frame (Khairallah and Kassas, 2021). Even sophisticated high-fidelity numerical propagators incorporating complex force models, which showed improved propagation accuracy, require prior knowledge of force parameters that are not publicly available (Vallado, 2005; Hough, 2014; Jones and Weisman, 2019).

Modeling orbit errors has been studied recently for improved opportunistic PNT with LEO satellites. Precise orbit determination and LEO navigation augmentation were proposed to achieve GNSS-like positioning (Michalak et al., 2021; Meng et al., 2021); however, access to a GNSS receiver onboard the LEO SVs would be needed, posing additional challenges. An orbit error compensation method was introduced in (Wang et al., 2023) to improve Doppler positioning accuracy.

Differential navigation offers an alternative technique to correct for satellite orbit, atmospheric, and clock errors (Yan and Zhang, 2022; Jiang et al., 2023b). This technique consists of a base station with a known position, listening to the same satellites as a navigating rover with an unknown state. The base station transmits measurement corrections to the rover (Parkinson and Enge, 1996; Hwang et al., 1999). At a sufficiently small baseline distance, differenced measurements from the two receivers significantly reduce the aforementioned common mode errors mentioned. LEO-based differential navigation was studied using carrier phase measurements from Orbcomm (Khalife and Kassas, 2019; Khalife et al., 2020), and Doppler observables from Starlink (Neinavaie et al., 2022; Saroufim et al., 2023) and Iridium (Zhao et al., 2023). A recent study involving a multi-constellation differential simultaneous tracking and navigation (D-STAN) framework using differenced Doppler measurements from Starlink, OneWeb, Orbcomm, and Iridium SVs showed promisingly accurate navigation performance, achieving meter-level accuracy over a trajectory of about a kilometer (Kassas et al., 2023b).

This paper analyzes the dominating along-track error in the LEO SVs orbit and maps this error to the ranging error as seen by a ground-based receiver. It also analyzes the substantial benefit of the differential framework to reduce this error. This paper makes the following contributions. First, the pseudorange measurement model is presented for the non-differential and differential frameworks, and the propagation of ephemeris error onto the measurement model is derived. The analysis is conducted first in the SV's orbital plane for the non-differential framework, showing the effect of receiver-to-SV orientation on the measurement error and receiver localization. The analysis is then extended to the differential scenario, where the receiver-to-SV orientation is shown to hold a major impact on the differential error. Next, a numerical simulation study is presented, demonstrating the efficacy of differential navigation in reducing the effect of LEO ephemeris error on the navigation solution. The simulation considered an aerial vehicle equipped with a tactical-grade IMU, an altimeter, and a LEO satellites receiver listening to 14 Starlink and 11 OneWeb satellites, while a base station communicates its pseudorange measurements from the same LEO SVs to help with the measurement error corrections and improve the rover navigation performance. The rover traveled a distance of 28 km in 300 seconds, where GNSS signals were available for the first 60 seconds. The proposed framework achieved a position three-dimensional (3-D) root mean-squared error (RMSE) of 52 cm. Finally, experimental results are presented for a ground vehicle navigating for 540 m in 60 s with differential Doppler measurement from 2 Orbcomm and 1 Iridium NEXT LEO satellites, achieving a 3-D position RMSE of 7.13 m, despite using erroneous LEO SV ephemerides obtained from TLE+SGP4.

The rest of the paper is organized as follows: Section II presents the non-differential and differential measurement models. Section III shows the effect of ephemeris error on the range measurements. Section IV discusses the simulation results of a LEO-aided differential navigation. Section V shows experimental results validating the benefit of differential navigation. Section VI gives concluding remarks.

II. MODEL DESCRIPTION

This section presents the LEO satellites' pseudorange measurement model in both differential and non-differential frameworks.

1. Non-Differential Measurement Model

Pseudorange measurements ρ from a LEO satellite l extracted by a LEO receiver at time-step k, representing discrete-time instant $t_k = kT + t_0$, is modeled as

$$\rho_l(k) \;=\; \|\boldsymbol{r}_r(k) - \boldsymbol{r}_{leo,l}(k')\|_2 + c\cdot[\delta t_r(k) - \delta t_{leo,l}(k')] + c\delta t_{trop,l}(k) + c\delta t_{iono,l}(k) + \epsilon_{\rho,l}(k),$$

where k' represents discrete-time at $t_{k'} = kT + t_0 - \delta t_{TOF}$, with δt_{TOF} being the true time-of-flight of the signal from the LEO satellite to the receiver; $\boldsymbol{r}_r$ and $\boldsymbol{r}_{leo,l}$ are the 3-D position vectors of the receiver and the l-th LEO SV in the Earth-centered-Earth-fixed (ECEF) reference frame; c is the speed of light; δt_r and $\delta t_{leo,l}$ are the clock biases of the receiver and the l-th LEO SV, respectively; $\delta t_{iono,l}(k)$ and $\delta t_{trop,l}(k)$ are the ionospheric and tropospheric delays from the l-th LEO SV to the receiver at time-step k, respectively; and $\epsilon_{\rho,l}$ is the pseudorange measurement noise, which is modeled as a discrete-time zero-mean white Gaussian sequence with variance $\sigma^2_{\rho,l}(k)$.

2. Differential Measurement Model

The differential pseudorange measurement model across the rover R and the base B is defined as

$$\begin{aligned} z_l^{(R,B)}(k) \;&=\; \rho_l^{(R)}(k) - \rho_l^{(B)}(k) \\ &= \|\boldsymbol{r}_{r,R}(k) - \boldsymbol{r}_{leo,l}(k')\|_2 - \|\boldsymbol{r}_{r,B}(k) - \boldsymbol{r}_{leo,l}(k')\|_2 + c\delta t_r^{(R,B)}(k) + c\delta t_{trop,l}^{(R,B)}(k) + c\delta t_{iono,l}^{(R,B)}(k) + \epsilon_{\rho,l}^{(R,B)}(k), \end{aligned}$$

where

$$\begin{aligned} \delta t_r^{(R,B)}(k) \;&\triangleq\; \delta t_r^{(R)}(k) - \delta t_r^{(B)}(k) \\ \epsilon_{\rho,l}^{(R,B)}(k) \;&\triangleq\; \epsilon_{\rho,l}^{(R)}(k) - \epsilon_{\rho,l}^{(B)}(k). \end{aligned}$$

III. EFFECT OF EPHEMERIS ERROR ON LEO SATELLITES MEASUREMENTS

Each satellite is characterized by its orbital plane, where its motion along the orbit is defined by the rate of change in its true anomaly. Therefore, a satellite state error that is concentrated in the along-track axis in a low eccentricity orbit can be represented as a true anomaly angle error. To assess the error at this level, a theoretical analysis is conducted in the satellite's orbital plane, where exact relations can be derived and generalized for all LEO SVs' orbits. This section addresses the LEO SV state errors reflected in the range measurement for the non-differential and differential configurations.

1. Non-Differential Framework

Define $\hat{\boldsymbol{r}}_{leo,l}$, $\hat{\dot{\boldsymbol{r}}}_{leo,l}$ as the estimated "erroneous" position and velocity of the l^{th} LEO satellite extracted from the TLEs; $\hat{\rho}_l$ is the corresponding pseudorange measurement; $\boldsymbol{r}_l$ and $\hat{\boldsymbol{r}}_l$ are the range vectors from the receiver to the l^{th} true and estimated LEO SV, respectively. To study the impact of the LEO satellite state error on the pseudorange, for simplicity, perfect clocks are assumed. Hence, the range error ν can be written as

$$\begin{aligned} \nu &= \rho_l - \hat{\rho}_l \\ &= \|\boldsymbol{r}_l\| - \|\hat{\boldsymbol{r}}_l\| \\ &= \|\boldsymbol{r}_r - \boldsymbol{r}_{leo,l}\| - \|\boldsymbol{r}_r - \hat{\boldsymbol{r}}_{leo,l}\|. \end{aligned}$$

Given that most of the state error resides in the satellite's in-track direction, it is beneficial to study this effect in each satellite's orbital plane, where all SVs would behave similarly regardless of their orbital elements. Figure 1 illustrates the orbital plane of satellite l with the projection of the receiver position vector onto this plane. Define $\boldsymbol{e}$ to be the error vector of a LEO satellite in its orbital plane, namely

$$\begin{aligned} \boldsymbol{e} &= \hat{\boldsymbol{r}}_{leo,l} - \boldsymbol{r}_{leo,l} \\ &= \hat{\boldsymbol{r}}_l - \boldsymbol{r}_l. \end{aligned}$$

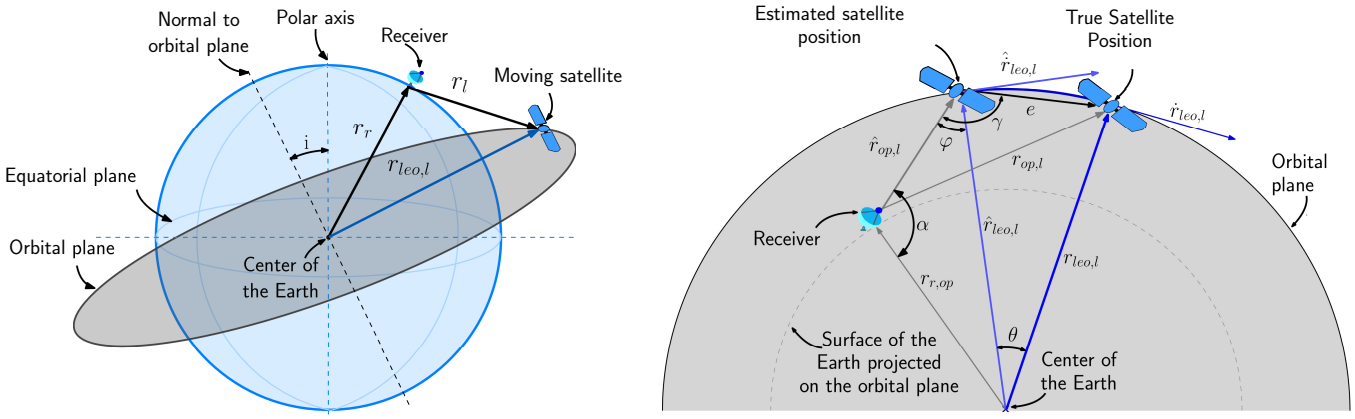

Figure 1: Earth and satellite's orbit (left). Orbital plane for a non-differential scenario: estimated and actual LEO satellite positions with corresponding range measurements to a stationary receiver projected onto the satellite's orbital plane (right).

Denote a variable 'a' as the L2 norm of its corresponding vector form, i.e., $a = \|\boldsymbol{a}\|$. Also, let $\boldsymbol{r}_{op,l}$, $\hat{\boldsymbol{r}}_{op,l}$, and $\boldsymbol{r}_{r,op}$ represent the projections of $\boldsymbol{r}_l$, $\hat{\boldsymbol{r}}_l$, and $\boldsymbol{r}_r$, respectively, on the l^{th} LEO satellite's orbital plane. Hence, the true orbital plane range can be written as

$$r_{op} = \sqrt{\hat{r}_{op}^2 + e^2 - 2\hat{r}_{op}.\cos\gamma}.$$

Assuming a circular orbit for a small in-track error e, leads to $\hat{r}_{leo} \approx r_{leo}$. From Figure 1, it can be seen that γ can be written as

$$\gamma = \varphi + \frac{\pi - \theta}{2}.$$

Knowing that the along-track error e is at the order of few kilometers, and the magnitude of the LEO satellite's position vector in the ECEF coordinate system, $\hat{r}_{leo}$ is in the range $6550 - 7500$ km, resulting in a true anomaly error $\theta \approx 0.01°$, making the assumption $\cos\gamma \approx \sin\varphi$ valid. Taking the satellite position error to be along the direction of motion, the range error can be written as $\nu = |r_{op} - \hat{r}_{op}|$, where the only variable is φ, leading to

$$\nu = \hat{r}_{op}\left(\sqrt{1 \pm \frac{2.e.\sin\varphi}{\hat{r}_{op}}} - 1\right). \tag{1}$$

Without prior knowledge of the ephemeris, it is difficult to estimate the magnitude of the SV state error. To circumvent this, a differential framework is adapted to reduce the effect of SV ephemeris error on the navigation solution.

2. Differential Framework

This subsection analyzes the effect of a satellite ephemeris error at a single time epoch on the differential range measurements from two stationary receivers. A fixed baseline is assumed to study the impact of the orientation of two receivers with respect to the satellite on the differential range measurements subjected to orbital errors.

Let r_{r_i} and b denote the projection of the i^{th} receiver position and baseline onto the LEO satellite orbital plane, respectively, as illustrated in Figure 2. Following (1), the true range and range residual ν in the orbital plane can be calculated as

$$r_i = \hat{r}_i \left(\sqrt{1 + \frac{2.e.\sin\varphi_{r_i}}{\hat{r}_i}} \right)$$

$$\nu = \hat{r}_1 \left(\sqrt{1 + \frac{2.e.\sin\varphi_{r_1}}{\hat{r}_1}} - 1 \right) - \hat{r}_2 \left(\sqrt{1 + \frac{2.e}{\hat{r}_2}.\sin\left(\varphi_{r_1} - \varphi_{r_1,r_2}\right)} - 1 \right), \tag{2}$$

where the first and second terms in (2) represent the range errors at the first and second receivers, respectively, and

$$\varphi_{r_{r_1,r_2}} = \arccos\left(\frac{\hat{r}_1^2 + \hat{r}_2^2 - b^2}{2\hat{r}_1\hat{r}_2} \right).$$

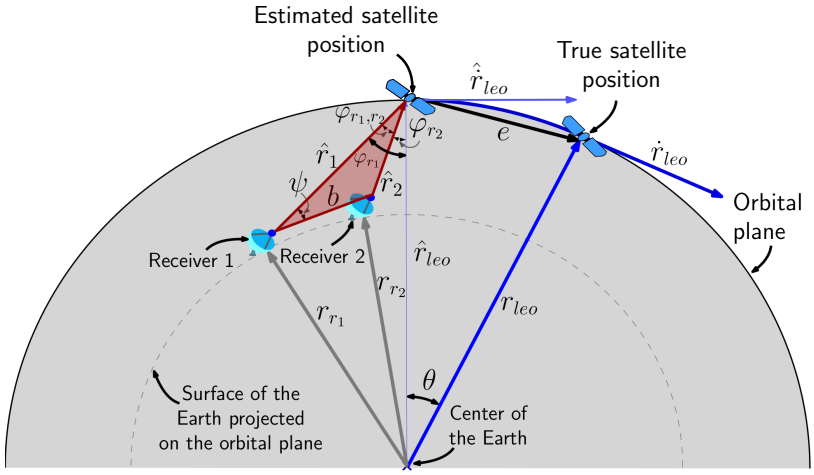

Figure 2: Differential scenario in the orbital plane: estimated and actual LEO satellite positions with corresponding range measurements to two stationary receivers projected onto the satellite's orbital plane.

Fixing receiver 1 and the orbital plane baseline b, receiver 2 may take any position along the circle centered at receiver 1 with radius b. Hence, the only variable affecting the differential residual becomes $\varphi_{r_{r_1,r_2}}$, revealing the relationship between the orientation of the second receiver and measurement error at a specific time step. It can be shown from (2) that the error at the second receiver eliminates its counterpart on the first receiver when $\varphi_{r_{r_1,r_2}}$ is zero, while the largest residual error occurs when $\varphi_{r_{r_1,r_2}}$ is maximum, i.e., when $|\psi| = \frac{\pi}{2}$, which is the angle between the estimated range at the fixed receiver and the baseline.

A simulation was conducted to demonstrate these relationships. A receiver was placed at The Ohio State University, Columbus, Ohio, USA, and was assumed to listen to a Starlink LEO satellite, producing an estimated range measurement. The second receiver was moved along 100 different locations centered at the first receiver, with a radius of 5 km, shown in Figure 3(a). The true satellite position was simulated with a 4 km in-track error along the direction of motion, where the true reference range measurement was obtained. The two receivers listened to the same SV at each epoch, and the measurements were differenced at the estimated and true satellite positions for every baseline orientation. The differential residuals at each location of the second receiver are shown in Figure 3(b) studied in the satellite's orbital plane, where the maximum differential error was recorded when the baseline is normal to the projected estimated range vector on the orbital plane. The maximum differential residual for

a 4 km in-track error and 5 km baseline with the Starlink LEO satellite used was found to be 23 m, while almost zero differential residual is achieved when the baseline is co-linear with the projected estimated range vector at the fixed receiver.

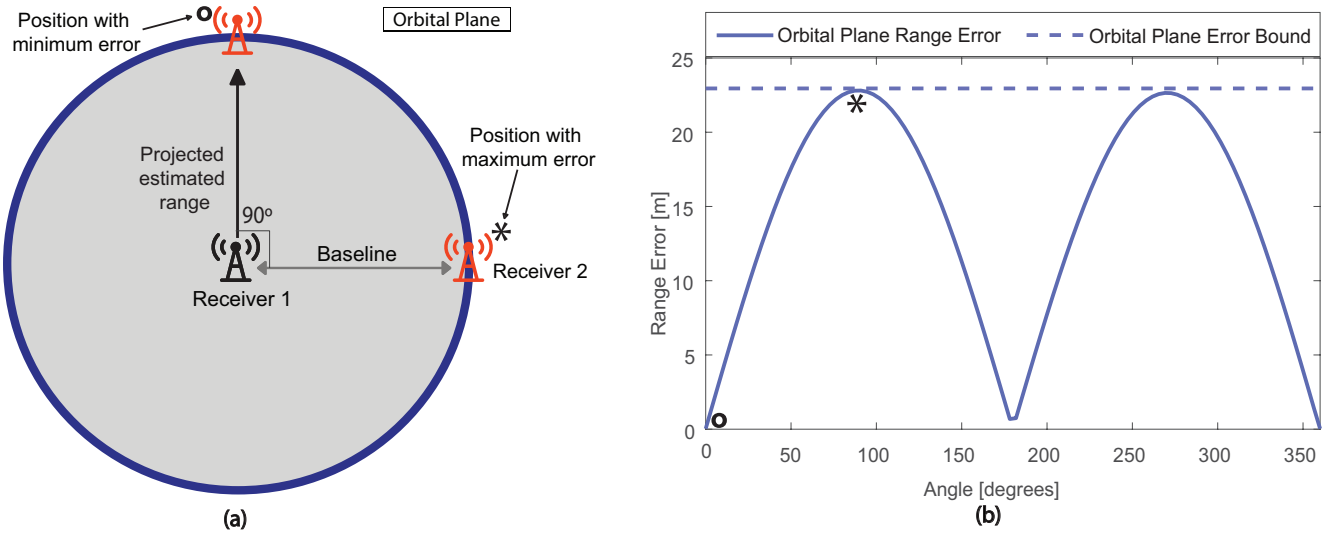

Figure 3: (a) Baseline orientation showing the locations of maximum and minimum differential range errors. (b) Differential range error and maximum range error with varying receivers-SV orientation in the orbital plane.

IV. SIMULATION OF DIFFERENTIAL NAVIGATION WITH LEO SATELLITES

This section presents simulation results of a differential framework comprising a moving rover with unknown states and a stationary basestation with a known position. The rover and base make pseudorange measurements to L LEO satellites, where the base communicates its position, pseudorange measurements, and measurement noise variance $\sigma^{2}_{\rho,l}{}^{(B)}$ to the rover. Figure 4 depicts a block diagram of the differential framework adapted by the rover, where IMU measurements are tightly coupled with GNSS and LEO pseudoranges via an extended Kalman filter (EKF). The following subsections formulate the EKF and present the EKF error plots.

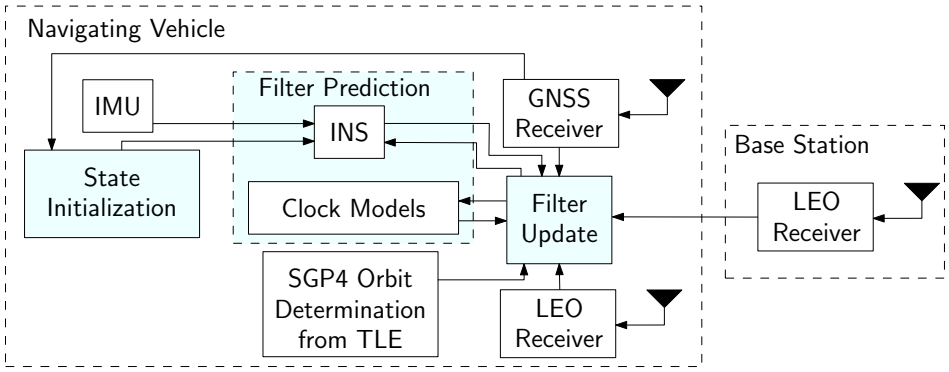

Figure 4: LEO-aided INS differential framework

1. EKF Formulation

The EKF for the differential framework shown in Figure 4 is implemented to estimate the moving rover's states and clock state difference between the base and rover. The state vector is defined as

$$\begin{aligned} \boldsymbol{x} &= [\boldsymbol{x}_r{}^{\mathsf{T}},\, \boldsymbol{x}_{clk}{}^{\mathsf{T}}]^{\mathsf{T}} \\ \boldsymbol{x}_r &= [{}^{b}_{g}\bar{\boldsymbol{q}}^{\mathsf{T}},\, \boldsymbol{r}_r^{\mathsf{T}},\, \dot{\boldsymbol{r}}_r^{\mathsf{T}},\, \boldsymbol{b}_{gyr}^{\mathsf{T}},\, \boldsymbol{b}_{acc}^{\mathsf{T}}]^{\mathsf{T}} \\ \boldsymbol{x}_{clk} &= [c\delta t_r^{(R,B)}, c\dot{\delta} t_r^{(R,B)}] \end{aligned}$$

where $\boldsymbol{x}_r$ is the vehicle's state vector, composed of ${}^{b}_{g}\bar{\boldsymbol{q}}$, which is a four-dimensional unit quaternion representing the orientation of the body frame $\{b\}$ fixed at the inertial navigation system (INS) with respect to the global frame $\{g\}$; $\boldsymbol{r}_r$ and $\dot{\boldsymbol{r}}_r$ are the 3-D position and velocity of the vehicle expressed in $\{g\}$; and $\boldsymbol{b}_{gyr}$ and $\boldsymbol{b}_{acc}$ are the 3-D biases of the IMU's gyroscope and accelerometer, respectively, expressed in $\{\mathrm{b}\}$. The vector $\boldsymbol{x}_{clk}$ is the clock state, composed of the difference between the rover and the base clock bias and drift. The IMU and clock dynamics models are detailed in (Saroufim et al., 2023), whereas the strap-down INS kinematic equations used to estimate the orientation, position, and velocity of the rover can be found in (Kassas et al., 2023a).

2. Simulation

The simulation environment comprised a stationary receiver located at the Electroscience Laboratory, at The Ohio State University, Columbus, Ohio, USA. The base was equipped with a LEO receiver producing pseudorange measurements to 14 Starlink and 11 OneWeb LEO SVs. A fixed-wing aerial vehicle was simulated to fly for 300 seconds over Columbus, traveling a total distance of 28 km. The vehicle was equipped with a tactical-grade IMU, an altimeter, a GNSS receiver, and an opportunistic LEO receiver making pseudorange measurements to the same 25 LEO satellites. For the first 60 seconds, GNSS and altimeter measurements were fused in a loosly coupled fashion to aid the onboard INS, before cutting off GNSS signals for the remaining 240 seconds. After GNSS cutoff, the aerial vehicle fused altimeter, Starlink, and OneWeb LEO pseudorange measurements, along with the communicated pseudoranges from the base-station to navigate the rover. The gyroscope and accelerometer readings were simulated from the vehicle's kinematics as explained in (Saroufim et al., 2023). The two receivers were equipped with a high-quality oven-controlled crystal oscillator (OCXO) clocks. Finally, the LEO satellites' ephemerides were generated via the Analytical Graphics Inc. (AGI) System Tool Kit (STK) and propagated using High Precision Orbit Propagator (HPOP) with an elevation mask of 15 degrees.

Table 1: Simulation Environment.

Metric	Total	No GNSS
Distance [km]	28	23
Time [s]	300	240

Figure 5 illustrates the LEO SVs' trajectories and the aerial vehicle trajectories: ground truth, GNSS-aided INS, non-differential LEO-aided INS, and differential LEO-aided INS, while Figure 6 shows the EKF error plots. Note that the GNSS-INS error bounds diverge rapidly after GNSS-cutoff, and hence are not shown in the EKF plots. Tables 1 and 2 summarize the results.

The geometric and orbital diversity of Starlink and OneWeb shown in Fig. 5 reduce the position dilution of precision (PDOP) in the east and north directions, causing the vehicle's states to remain observable in these directions. The error convergence in the up direction is mainly due to the presence of altimeter corrections throughout the simulation period. These results present the potential of a sub-meter accuracy with a differential LEO-aided INS navigation, and the significant reduction of common mode errors including ephemeris and clock effects.

Table 2: Simulation results.

Framework	2-D position RMSE [m]	Final error [m]
GNSS-INS	528	1,795
Non-differential LEO-aided INS	12.5	7.1
Differential LEO-aided INS	0.52	0.10

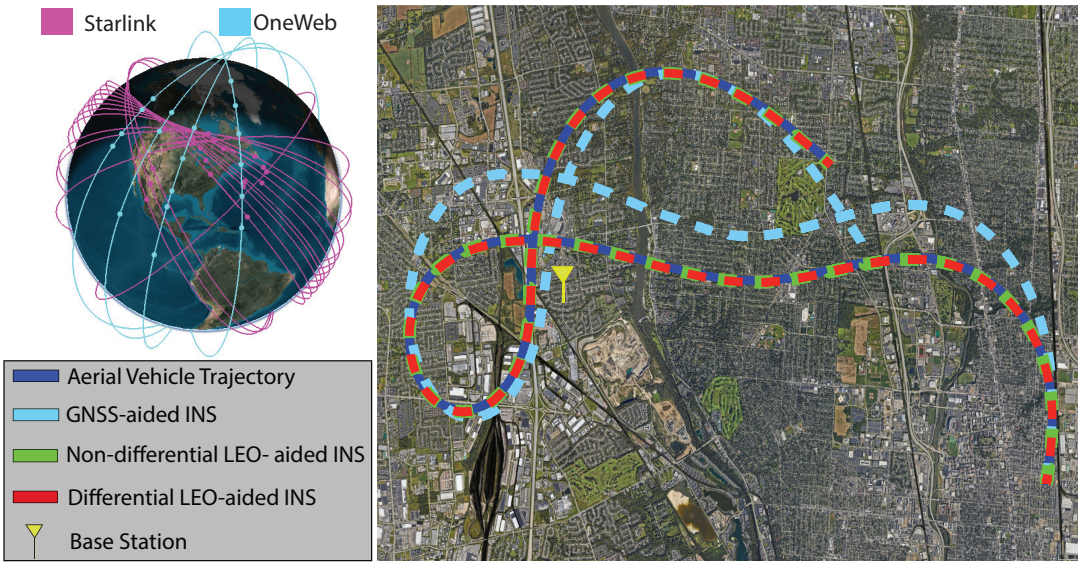

Figure 5: Simulation results showing the aerial vehicle trajectory, estimated trajectory with GNSS-aided INS, non-differential LEO-aided INS, and differential LEO-aided INS, as well as the SVs' trajectories used in the study.

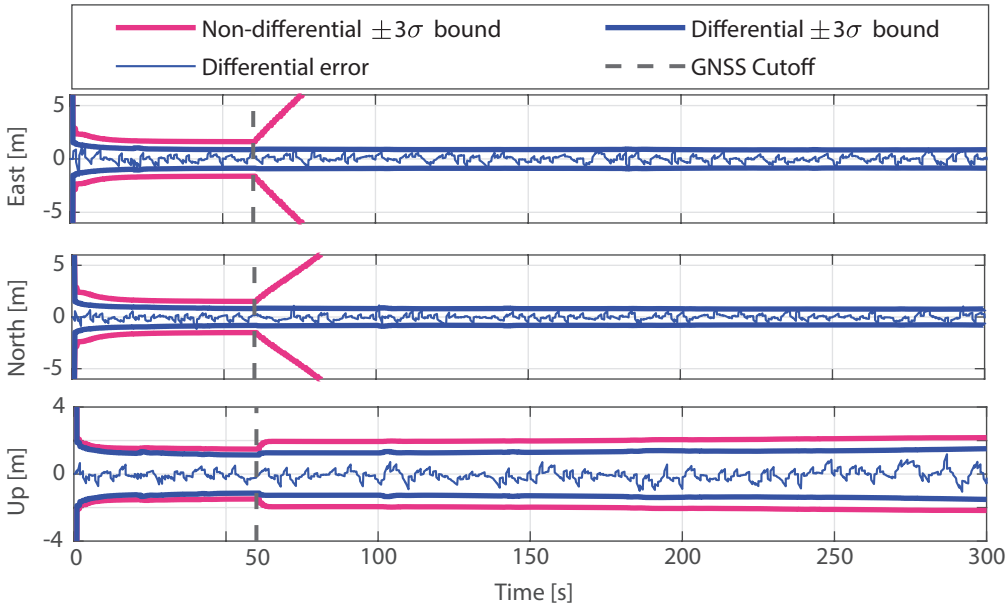

Figure 6: EKF estimation error plots and $\pm 3\sigma$ bounds of the aerial vehicle position for differential and non-differential LEO-aided INS in the ENU frame.

V. EXPERIMENTAL RESULTS

This section demonstrates the significance of differential navigation with LEO satellites experimentally. A ground vehicle navigated with Doppler measurements from 2 Orbcomm and 1 Iridium NEXT LEO SVs. Note since pseudorange measurements were not available from these LEO SVs, Doppler measurements were used instead. The vehicle's ground truth was obtained from a Septentrio AsteRx SBi3 Pro+ integrated GNSS-INS system with real-time kinematic (RTK), and using an industrial-grade IMU. The vehicle traveled a total distance of 540 m in 60 seconds in Columbus, Ohio, USA, while a differential base-station with known position was installed on top of the ElectroScience Laboratory, at The Ohio State University, with a mean baseline distance of 1.1 km from the ground vehicle (see Fig. 7). During the experiment, the LEO receivers on the base and ground vehicle were listening to the same 3 SVs. GNSS signals were available for the first 20 seconds, then made virtually unavailable for the remaining 40 seconds, during which the vehicle traversed 492 m.

Table 3: Trajectory settings

Metric	Total	No GNSS
Distance [km]	0.54	0.492
Time [s]	60	40

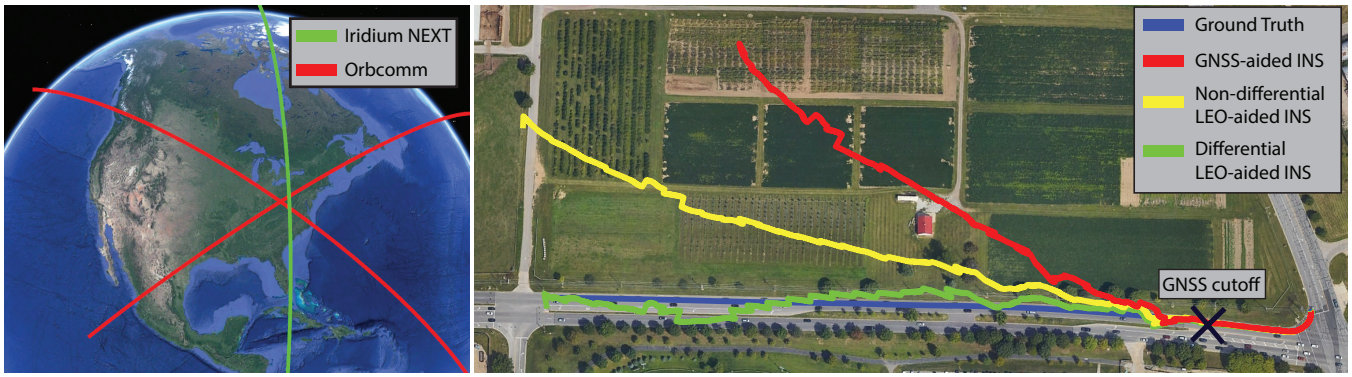

Figure 7: Experimental results showing Orbcomm and Iridium LEO SVs' trajectories (left), and the navigating vehicle's trajectory, GNSS-aided INS trajectory, non-differential LEO-aided INS, and differential LEO-aided INS (right).

To demonstrate the benefit of differential navigation with LEO satellites, the ground vehicle's attitude, 3-D position and velocity were estimated and compared to: (i) non-differential LEO-aided INS and (ii) GNSS-aided INS where the vehicle relies solely on the IMU measurements after GNSS signals were cut off. Fig. 7 shows the vehicle's true trajectory, GNSS-aided INS, non-differential LEO-aided INS, and differential LEO-aided INS. Tables 3 and 4 summarize the results.

Table 4: Experimental results

Framework	2-D position RMSE [m]	Final error [m]
GNSS-INS	87.74	212.53
Non-differential LEO-aided INS	41.29	112.56
Differential LEO-aided INS	7.13	5.38

VI. CONCLUSION

This paper analyzed the effect of the dominating along-track ephemeris error on the orbital plane range measurement error for a fixed base-station. The study was then extended to the differential framework, showing that the differential range error due to ephemeris bias is closely related to the receiver-to-SV orientation. A simulation study was conducted to evaluate the performance of the differential framework using pseudorange measurements from 14 Starlink and 11 OneWeb LEO SVs. The results showed a 3-D position RMSE of 52 cm along a 28 km trajectory, compared to 12.5 m using the non-differential framework. Finally, experimental results of a moving ground vehicle using Doppler measurements from 2 Orbcomm and 1 Iridium SVs reduced the position RMSE from 87.74 m using GNSS-aided INS, and 41.29 m using non-differential LEO-aided INS, to 7.13 m with the proposed differential LEO-aided INS framework.

ACKNOWLEDGEMENTS

This work was supported in part by the Office of Naval Research (ONR) under Grant N00014-19-1-2511, in part by the Air Force Office of Scientific Research (AFOSR) under Grant FA9550-22-1-0476, in part by the U.S. Department of Transportation (USDOT) under Grant 69A3552047138, and in part by The Aerospace Corporation under Award 4400000428. The authors would like to thank Sharbel Kozhaya and Haitham Kanj for their help in experimental data collection and processing.

REFERENCES

Bhatti, J. and Humphreys, T. (2017). Hostile control of ships via false GPS signals: Demonstration and detection. *NAVIGATION, Journal of the Institute of Navigation*, 64(1):51–66.

Bilardi, S. (2021). A GNSS signal simulator and processor for evaluating acquisition and tracking of GPS-like signals from satellites in LEO. Master's thesis, University of Colorado at Boulder, CO, USA.

Cassel, R., Scherer, D., Wilburne, D., Hirschauer, J., and Burke, J. (2022). Impact of improved oscillator stability on LEO-based satellite navigation. In *Proceedings of ION International Technical Meeting*, pages 893–905.

Egea-Roca, D., Lopez-Salcedo, J., Seco-Granados, G., and Falletti, E. (2022). Performance analysis of a multi-slope chirp spread spectrum signal for PNT in a LEO constellation. In *Proceedings of Workshop on Satellite Navigation Technology*, pages 1–9.

Farhangian, F., Benzerrouk, H., and Landry, R. (2021). Opportunistic in-flight INS alignment using LEO satellites and a rotatory IMU platform. *Aerospace*, 8(10):280–281.

Farhangian, F. and Landry, R. (2023). High-order pseudorange rate measurement model for multi-constellation LEO/INS integration: Case of Iridium-NEXT, Orbcomm, and Globalstar. *Proceedings of the Institution of Mechanical Engineers, Part G: Journal of Aerospace Engineering*, 237(4):925–939.

Guo, F., Yang, Y., Ma, F., Liu, Y. Z. H., and Zhang, X. (2023). Instantaneous velocity determination and positioning using doppler shift from a LEO constellation. *Satellite Navigation*, 4:9–21.

Hartnett, M. (2022). Performance assessment of navigation using carrier Doppler measurements from multiple LEO constellations. Master's thesis, Air Force Institute of Technology, Ohio, USA.

Hegarty, C., Bobyn, D., Grabowski, J., and Van Dierendonck, A. (2020). An overview of the effects of out-of-band interference on GNSS receivers. *NAVIGATION, Journal of the Institute of Navigation*, 67(1):143–161.

Hough, M. (2014). Closed-form nonlinear covariance prediction for two-body orbits. *Journal of Guidance, Control, and Dynamics*, 37(1):26–35.

Huang, C., Qin, H., Zhao, C., and Liang, H. (2022). Phase - time method: Accurate Doppler measurement for Iridium NEXT signals. *IEEE Transactions on Aerospace and Electronic Systems*, 58(6):5954–5962.

Humphreys, T., Iannucci, P., Komodromos, Z., and Graff, A. (2023). Signal structure of the Starlink Ku-band downlink. *IEEE Transactions on Aerospace and Electronics Systems*. accepted.

Hwang, P., McGraw, G., and Bader, J. (1999). Enhanced differential GPS carrier-smoothed code processing using dual-frequency measurements. *NAVIGATION, Journal of the Institute of Navigation*, 46(2):127–138.

Janssen, T., Koppert, A., Berkvens, R., and Weyn, M. (2023). A survey on IoT positioning leveraging LPWAN, GNSS and LEO-PNT. *IEEE Internet of Things Journal*, 10(13):11135–11159.

Jardak, N. and Jault, Q. (2022). The potential of LEO satellite-based opportunistic navigation for high dynamic applications. *Sensors*, 22(7):2541–2565.

Jiang, M., Qin, H., Su, Y., Li, F., and Mao, J. (2023a). A design of differential-low Earth orbit opportunistically enhanced GNSS (D-LoeGNSS) navigation framework. *Remote Sensing*, 15(8):2136–2158.

Jiang, M., Qin, H., Su, Y., Li, F., and Mao, J. (2023b). A design of differential-low Earth orbit opportunistically enhanced GNSS (D-LoeGNSS) navigation framework. *Remote Sensing*, 15(8):1–23.

Jiang, M., Qin, H., Zhao, C., and Sun, G. (2022). LEO Doppler-aided GNSS position estimation. *GPS Solutions*, 26(1):1–18.

Jones, B. and Weisman, R. (2019). Multi-fidelity orbit uncertainty propagation. *Acta Astronautica*, 155:406–417.

Kanamori, H., Kobayashi, K., and Kubo, N. (2023). A map-matching based positioning method using Doppler tracking and estimation by a software-defined receiver for multi-constellation LEO satellites. In *Proceedings of ION International Technical Meeting*, pages 649–663.

Kassas, Z., Khairallah, N., and Kozhaya, S. (2023a). Ad astra: Simultaneous tracking and navigation with megaconstellation LEO satellites. *IEEE Aerospace and Electronic Systems Magazine*. accepted.

Kassas, Z., Kozhaya, S., Kanj, H., Saroufim, J., Hayek, S., Neinavaie, M., Khairallah, N., and Khalife, J. (2023b). Navigation with multi-constellation LEO satellite signals of opportunity: Starlink, Oneweb, Orbcomm, and Iridium. In *Proceedings of IEEE/ION Position, Location, and Navigation Symposium*, pages 338–343.

Kassas, Z., Morales, J., and Khalife, J. (2019). New-age satellite-based navigation – STAN: simultaneous tracking and navigation with LEO satellite signals. *Inside GNSS Magazine*, 14(4):56–65.

Kassas, Z., Neinavaie, M., Khalife, J., Khairallah, N., Haidar-Ahmad, J., Kozhaya, S., and Shadram, Z. (2021). Enter LEO on the GNSS stage: Navigation with Starlink satellites. *Inside GNSS Magazine*, 16(6):42–51.

Kennewell, J. and Vo, B. (2013). An overview of space situational awareness. In *Proceedings of International Conference on Information Fusion*, pages 1029–1036.

Khairallah, N. and Kassas, Z. (2021). Ephemeris closed-loop tracking of LEO satellites with pseudorange and Doppler measurements. In *Proceedings of ION GNSS Conference*, pages 2544–2555.

Khalife, J. and Kassas, Z. (2019). Assessment of differential carrier phase measurements from Orbcomm LEO satellite signals for opportunistic navigation. In *Proceedings of ION GNSS Conference*, pages 4053–4063.

Khalife, J. and Kassas, Z. (2022). On the achievability of submeter-accurate UAV navigation with cellular signals exploiting loose network synchronization. *IEEE Transactions on Aerospace and Electronic Systems*, 58(5):4261–4278.

Khalife, J. and Kassas, Z. (2023). Performance-driven design of carrier phase differential navigation frameworks with mega-constellation LEO satellites. *IEEE Transactions on Aerospace and Electronic Systems*, 59(3):2947–2966.

Khalife, J., Neinavaie, M., and Kassas, Z. (2020). Navigation with differential carrier phase measurements from megaconstellation LEO satellites. In *Proceedings of IEEE/ION Position, Location, and Navigation Symposium*, pages 1393–1404.

Khalife, J., Neinavaie, M., and Kassas, Z. (2022). The first carrier phase tracking and positioning results with Starlink LEO satellite signals. *IEEE Transactions on Aerospace and Electronic Systems*, 56(2):1487–1491.

Kozhaya, S., Haidar-Ahmad, J., Abdallah, A., Kassas, Z., and Saab, S. (2021). Comparison of neural network architectures for simultaneous tracking and navigation with LEO satellites. In *Proceedings of ION GNSS Conference*, pages 2507–2520.

Maaref, M., Khalife, J., and Kassas, Z. (2019). Lane-level localization and mapping in GNSS-challenged environments by fusing lidar data and cellular pseudoranges. *IEEE Transactions on Intelligent Vehicles*, 4(1):73–89.

McGraw, G. and Braasch, M. (1999). GNSS multipath mitigation using gated and high resolution correlator concepts. In *Proceedings of ION National Technical Meeting*, pages 333–342.

Meng, L., Chen, J., Wang, J., and Zhang, Y. (2021). Broadcast ephemerides for LEO augmentation satellites based on nonsingular elements. *GPS Solutions*, 25(4):129–139.

Menzione, F. and Paonni, M. (2023). LEO-PNT mega-constellations: a new design driver for the next generation MEO GNSS space service volume and spaceborne receivers. In *Proceedings of IEEE/ION Position, Location, and Navigation Symposium*, pages 1196–1207.

Michalak, G., Glaser, S., Neumayer, K., and König, R. (2021). Precise orbit and earth parameter determination supported by LEO satellites, inter-satellite links and synchronized clocks of a future gnss. *Advances in Space Research*, 68(12):4753–4782.

Miralles, D., Bornot, A., Rouquette, P., Levigne, N., Akos, D., Y.-H.Chen, Lo, S., and Walter, T. (2020). An assessment of GPS spoofing detection via radio power and signal quality monitoring for aviation safety operations. *IEEE Intelligent Transportation Systems Magazine*, 12(3):136–146.

More, H., Cianca, E., and Sanctis, M. (2022). Positioning performance of LEO mega constellations in deep urban canyon environments. In *Proceedings of International Symposium on Wireless Personal Multimedia Communications*, pages 256–260.

Morton, Y., Xu, D., and Jiao, Y. (2022). Ionospheric scintillation effects on signals transmitted from LEO satellites. In *Proceedings of ION GNSS Conference*, pages 2980–2988.

Neinavaie, M., Shadram, Z., Kozhaya, S., and Kassas, Z. M. (2022). First results of differential Doppler positioning with unknown Starlink satellite signals. In *Proceedings of IEEE Aerospace Conference*, pages 1–14.

Orabi, M., Khalife, J., and Kassas, Z. (2021). Opportunistic navigation with Doppler measurements from Iridium Next and Orbcomm LEO satellites. In *Proceedings of IEEE Aerospace Conference*, pages 1–9.

Parkinson, B. and Enge, P. (1996). Differential GPS. *Global Positioning System: Theory and applications.*, 2:3–50.

Peral-Rosado, J., Lopez-Salcedo, J., Kim, S., and Seco-Granados, G. (2016). Feasibility study of 5G-based localization for assisted driving. In *Proceedings of International Conference on Localization and GNSS*, pages 1–6.

Pinell, C., Prol, F., Bhuiyan, M., and Praks, J. (2023). Receiver architectures for positioning with low earth orbit satellite signals: a survey. *EURASIP Journal on Advances in Signal Processing*, 2023:60–80.

Prol, F., Ferre, R., Saleem, Z., Välisuo, P., Pinell, C., Lohan, E., Elsanhoury, M., Elmusrati, M., Islam, S., Celikbilek, K., Selvan, K., Yliaho, J., Rutledge, K., Ojala, A., Ferranti, L., Praks, J., Bhuiyan, M., Kaasalainen, S., and Kuusniemi, H. (2022). Position, navigation, and timing (PNT) through low earth orbit (LEO) satellites: A survey on current status, challenges, and opportunities. *IEEE Access*, 10:83971–84002.

Prol, F., Kaasalainen, S., Lohan, E., Bhuiyan, M., Praks, J., and Kuusniemi, H. (2023). Simulations using LEO-PNT systems: A brief survey. In *Proceedings of IEEE/ION Position, Location, and Navigation Symposium*, pages 1381–387.

Psiaki, M. (2021). Navigation using carrier Doppler shift from a LEO constellation: TRANSIT on steroids. *NAVIGATION, Journal of the Institute of Navigation*, 68(3):621–641.

Ries, L., Limon, M., Grec, F., Anghileri, M., Prieto-Cerdeira, R., Abel, F., Miguez, J., Perello-Gisbert, J., d'Addio, S., R. Ioannidis and, A. O., Rapisarda, M., Sarnadas, R., and Testani, P. (2023). LEO-PNT for augmenting Europe's space-based PNT capabilities. In *Proceedings of IEEE/ION Position, Location, and Navigation Symposium*, pages 329–337.

Sabbagh, R. and Kassas, Z. (2023). Observability analysis of receiver localization via pseudorange measurements from a single LEO satellite. *IEEE Control Systems Letters*, 7(3):571–576.

Saroufim, J., Hayek, S., and Kassas, Z. (2023). Simultaneous LEO satellite tracking and differential LEO-aided IMU navigation. In *Proceedings of IEEE/ION Position Location and Navigation Symposium*, pages 179–188.

Shi, C., Zhang, Y., and Li, Z. (2023). Revisiting Doppler positioning performance with LEO satellites. *GPS Solutions*, 27(3):126–137.

Singh, U., Shankar, M., and Ottersten, B. (2022). Opportunistic localization using LEO signals. In *Proceedings of Asilomar Conference on Signals, Systems, and Computers*, pages 894–899.

Tan, Z., Qin, H., Cong, L., and Zhao, C. (2019). Positioning using IRIDIUM satellite signals of opportunity in weak signal environment. *Electronics*, 9(1):37.

Vallado, D. (2005). An analysis of state vector propagation using differing flight dynamics programs. In *Proceedings of the AAS Space Flight Mechanics Conference*, volume 120, pages 1563–1592.

Vallado, D. and Crawford, P. (2008). SGP4 orbit determination. In *Proceedings of AIAA/AAS Astrodynamics Specialist Conference and Exhibit*, pages 6770–6799.

Wang, D., Qin, H., and Huang, Z. (2023). Doppler positioning of LEO satellites based on orbit error compensation and weighting. *IEEE Transactions on Instrumentation and Measurement*, 72:1–11.

Wei, Q., Chen, X., and Zhan, Y. (2020). Exploring implicit pilots for precise estimation of LEO satellite downlink Doppler frequency. *IEEE Communications Letters*, 24(10):2270–2274.

Whiton, R., Chen, J., Johansson, T., and Tufvesson, F. (2022). Urban navigation with LTE using a large antenna array and machine learning. In *Proceedings of IEEE Vehicular Technology Conference*, pages 1–5.

Wu, N., Qin, H., and Zhao, C. (2023). Long-baseline differential doppler positioning using space-based SOP based on BPVGMM. *IEEE Transactions on Instrumentation and Measurement*, 72:1–10.

Yan, Z. and Zhang, X. (2022). Assessment of the performance of GPS/Galileo PPP-RTK convergence using ionospheric corrections from networks with different scales. *Earth, Planets and Space*, 74(1):1–19.

Yang, C. and Soloviev, A. (2023). Starlink Doppler and Doppler rate estimation via coherent combining of multiple tones for opportunistic positioning. In *Proceedings of IEEE/ION Position, Location, and Navigation Symposium*, pages 1143–1153.

Yang, C., Zang, B., Gu, B., Zhang, L., Dai, C., Long, L., Zhang, Z., Ding, L., and Ji, H. (2023). Doppler positioning of dynamic targets with unknown LEO satellite signals. *Electronics*, 12(11):2392–2404.

Ye, L., Gao, N., Yang, Y., Deng, L., and Li, H. (2023). Three satellites dynamic switching range integrated navigation and positioning algorithm with clock bias cancellation and altimeter assistance. *Aerospace*, 10(5):411–438.

Zhao, C., Qin, H., and Li, Z. (2022). Doppler measurements from multiconstellations in opportunistic navigation. *IEEE Transactions on Instrumentation and Measurement*, 71:1–9.

Zhao, C., Qin, H., Wu, N., and Wang, D. (2023). Analysis of baseline impact on differential doppler positioning and performance improvement method for LEO opportunistic navigation. *IEEE Transactions on Instrumentation and Measurement*, 72:1–10.